ACS OMEGA

http://pubs.acs.org/journal/acsodf

Article

# Nanostructured Indium Oxide Thin Films as a Room Temperature Toluene Sensor

Sunil Gavaskar Dasari, Pothukanuri Nagaraju,* Vijayakumar Yelsani, Sreekanth Tirumala, and Ramana Reddy M V

Cite This: *ACS Omega* 2021, 6, 17442−17454

Read Online

ACCESS | Metrics & More | Article Recommendations

**ABSTRACT:** Toluene gas is the most toxic and affects the respiratory system of humans, and thereby, its detection at lower levels is an important task. Herein, we report a room temperature-operatable indium oxide-based chemiresistive gas sensor, which detects 50 ppm toluene vapors. Nanocrystalline indium oxide ($In_2O_3$) films were sprayed on a pre-cleaned glass substrate using a cost-effective spray pyrolysis method at different substrate temperatures in the range of 350−500 °C. The X-ray diffraction studies confirmed that the sprayed thin films, which were deposited at different substrate temperatures, exhibit a cubic structure. The preferred orientation was aligned along the (222) orientation. Average crystallite size calculation based on the Scherrer formula indicates that the crystallite size increases with the enhancement of substrate temperature. FESEM analysis showed that the indium oxide thin films possess uniform grain distribution, which persists over the entire substrate. As the substrate temperature is increased, a partial agglomeration in the film morphology was observed. The deposited film's nanostructured nature was confirmed by transmission electron microscopy, and the polycrystalline nature was confirmed from the selected area electron diffraction pattern. Root mean square roughness of the samples was determined from the atomic force microscopy studies. From the Raman spectra, characteristic vibrational modes appeared at 558.61, 802.85, and 1097.18 $cm^{-1}$ in all the samples, which confirms the cubic structure of indium oxide thin films. Photoluminescence emission spectra have been recorded with an excitation wavelength of 280 nm. The optical band gap was measured using the Tauc plot. The band gap was found to decrease with an increase in the substrate temperature. The gas-sensing performance of indium oxide films sprayed at various substrate temperatures has demonstrated a better response toward 50 ppm toluene gas at room temperature with good stability, and the response and recovery times were determined using a transient response curve.

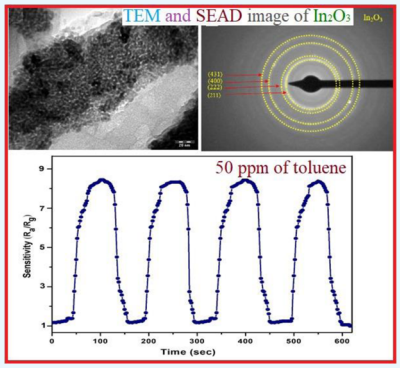


## INTRODUCTION

Metal oxide-based semiconductors have been widely investigated as sensing materials for a long time due to their abundant features, such as high sensitivity and selectivity toward volatile organic compounds.[1] Among them, indium oxide ($In_2O_3$) has been found to have pronounced sensitivity toward ammonia, methane, acetone, and other species due to its outstanding performance in electrical conductivity and due to abundant oxygen vacancies.[2,3] It is an n-type semiconductor with high stability and low specific resistance. Due to the direct band gap of ∼3.6 eV, it is a significant transparent conducting oxide material. It has received much attention in the fields of solar cells, optoelectronic devices, organic light-emitting diodes, photocatalysts, architectural glasses, field-emission catalysis, and sensors.[4−8] $In_2O_3$ has been prepared using thermal hydrolysis, the sol−gel technique, thermal decomposition, microemulsion, mechanical and chemical processing, pulsed laser deposition, and spray pyrolysis.[9−16] Among all the techniques described above, spray pyrolysis is a cost-effective and straightforward method. It has been investigated for the large-area deposition applications.

Gas sensors are designed to trace the low concentration of hazardous gases in the environment. These will play a vital role in many fields such as industrial control systems, household safety and security, fuel emission, and environmental pollution monitoring. Recently, various kinds of gas sensors are fabricated based on different sensing materials and their transduction principles. Among all the gas sensors, chemiresistive-type semiconducting metal oxide-based gas sensors are the essential materials to trace low concentrations of toxic gases such as benzene, xylene, acetone, ethylbenzene, toluene, and so forth. Among all these gases, toluene ($C_7H_8$) is the

Received: April 6, 2021
Accepted: June 23, 2021
Published: July 1, 2021

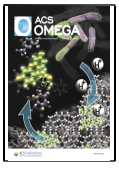





https://doi.org/10.1021/acsomega.1c01831
*ACS Omega* 2021, 6, 17442−17454

most harmful air pollutant with its wide range of applications as diluents and adhesive material in the decoration of interiors, which is firmly associated with our day-to-day lives and finally causes severe harm to human health with direct long-term exposure.[17] Consumption of toluene in low to moderate levels can cause weakness, tiredness, drunken-type actions, confusion, nausea, loss of appetite, memory and hearing loss, and even color vision loss. Few of these syndromes generally vanish when inhalation is impeded. Inhaling massive levels of toluene in a short time may cause unconsciousness, nausea, sleepiness, light headedness, and even death.[18] According to the suggestions of the OSHA, the short-term exposure limit of toluene is 100 ppm. It is associated with nasopharyngeal cancer, bronchial and chronic asthma, and other various subjective health problems. Also, toluene can be treated as an essential lung cancer biomarker.[19,20]

In this present work, an attempt was made to fabricate a cost-effective indium oxide sensor to trace low concentrations of toluene at room temperature.

## RESULTS AND DISCUSSION

**Thickness Measurement.** The thickness of the thin films deposited at different substrate temperatures is depicted in Figure 1. As the substrate temperature is increased, the thickness of the films is found to decrease. It may be due to the probability of the decomposition of the aerosol solution droplets near the preheated glass substrate, leading to a reduction in the particles' transportation in the direction of the substrate, and also, the sticking coefficient of an atom may be significantly less at higher substrate temperatures.[21]

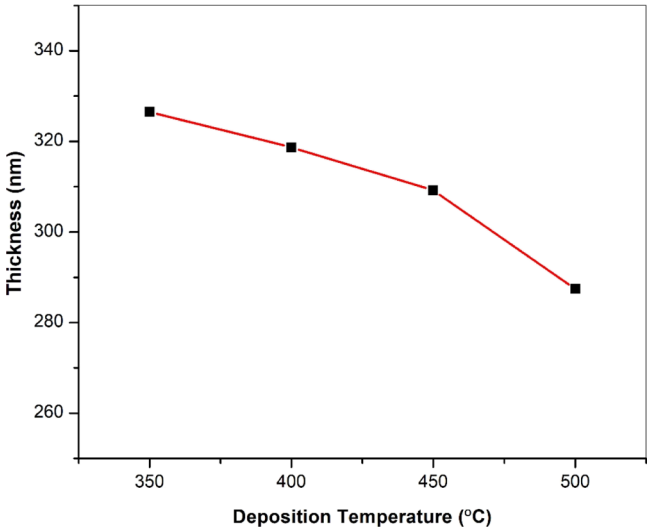


**Figure 1.** Variation of indium oxide thin-film thickness with substrate temperature.

**X-ray Diffraction.** The structural characterization of the indium oxide thin films sprayed at different substrate temperatures was studied using an X-ray diffractometer in a $2\theta$ range of 15−80°. The X-ray diffraction (XRD) patterns of indium oxide films are shown in Figure 2. It was noticed that indium oxide thin films are polycrystalline with a cubic structure without any additional impurities. All the diffraction peaks are listed using the Joint Committee on Powder Diffraction Standards, card no: 88-2160. The diffraction peaks appeared at 21.59, 30.66, 35.48, 45.78, 51.21, and 60.86, corresponding to (211), (222), (400), (431), (440), and (622) miller index planes, respectively. The intensity of the (222) peak is decreased with an increase in the substrate temperature. The average crystallite size has been calculated with Scherer's equation. The crystallite size increased with increasing substrate temperature, as shown in Figure 3. It might be due to the recrystallization process during the deposition[22]

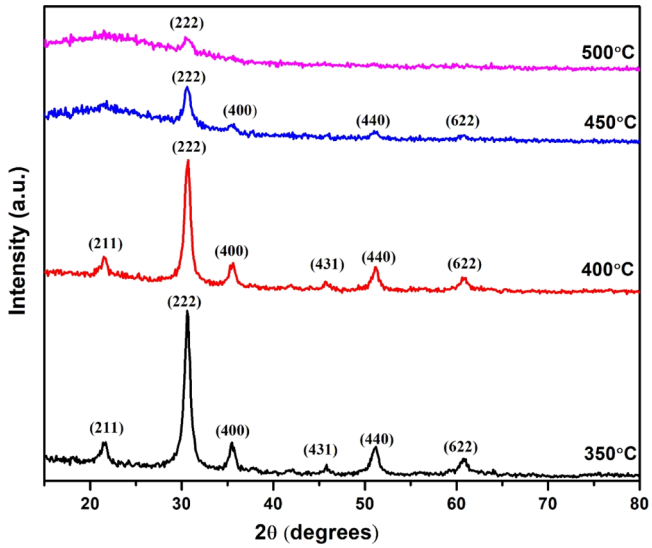


**Figure 2.** XRD spectra of $In_2O_3$ thin films.

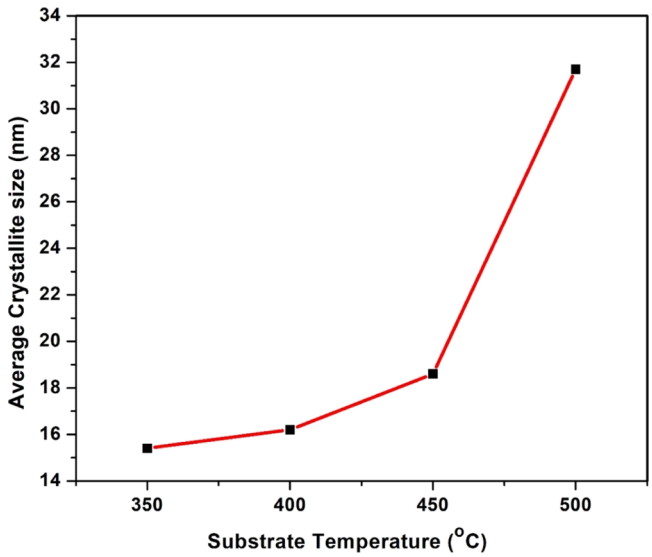


**Figure 3.** Average crystallite size of $In_2O_3$ thin films at different substrate temperatures.

$$\text{Average crystallite size } (D) = \frac{0.89\lambda}{\beta \cos\theta} \quad (1)$$

where "$\theta$" is the diffraction angle, "$\beta$" is full width at half maxima, and "$\lambda$" is the monochromatic X-ray wavelength.

The dislocation density ($\delta$) is defined as the length of dislocation lines per unit volume of the crystal and was determined using the following relation[23,24]



https://doi.org/10.1021/acsomega.1c01831
ACS Omega 2021, 6, 17442−17454

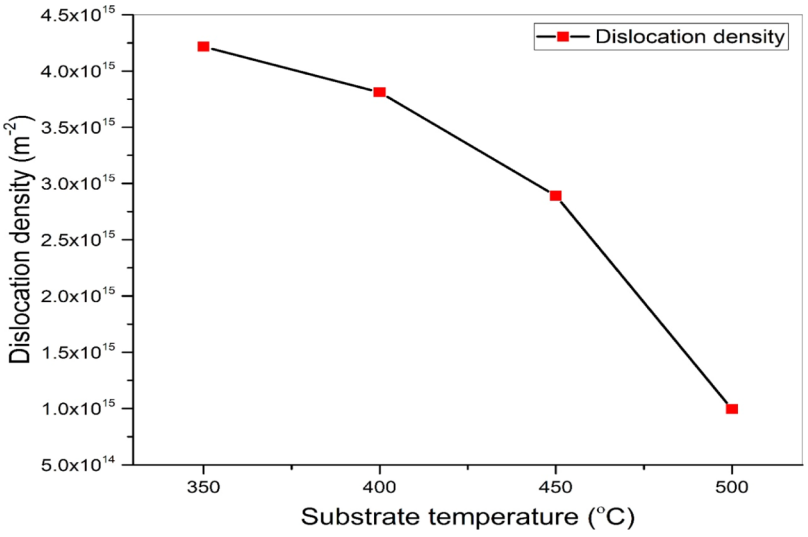


**Figure 4.** Dislocation density of the $In_2O_3$ thin films.

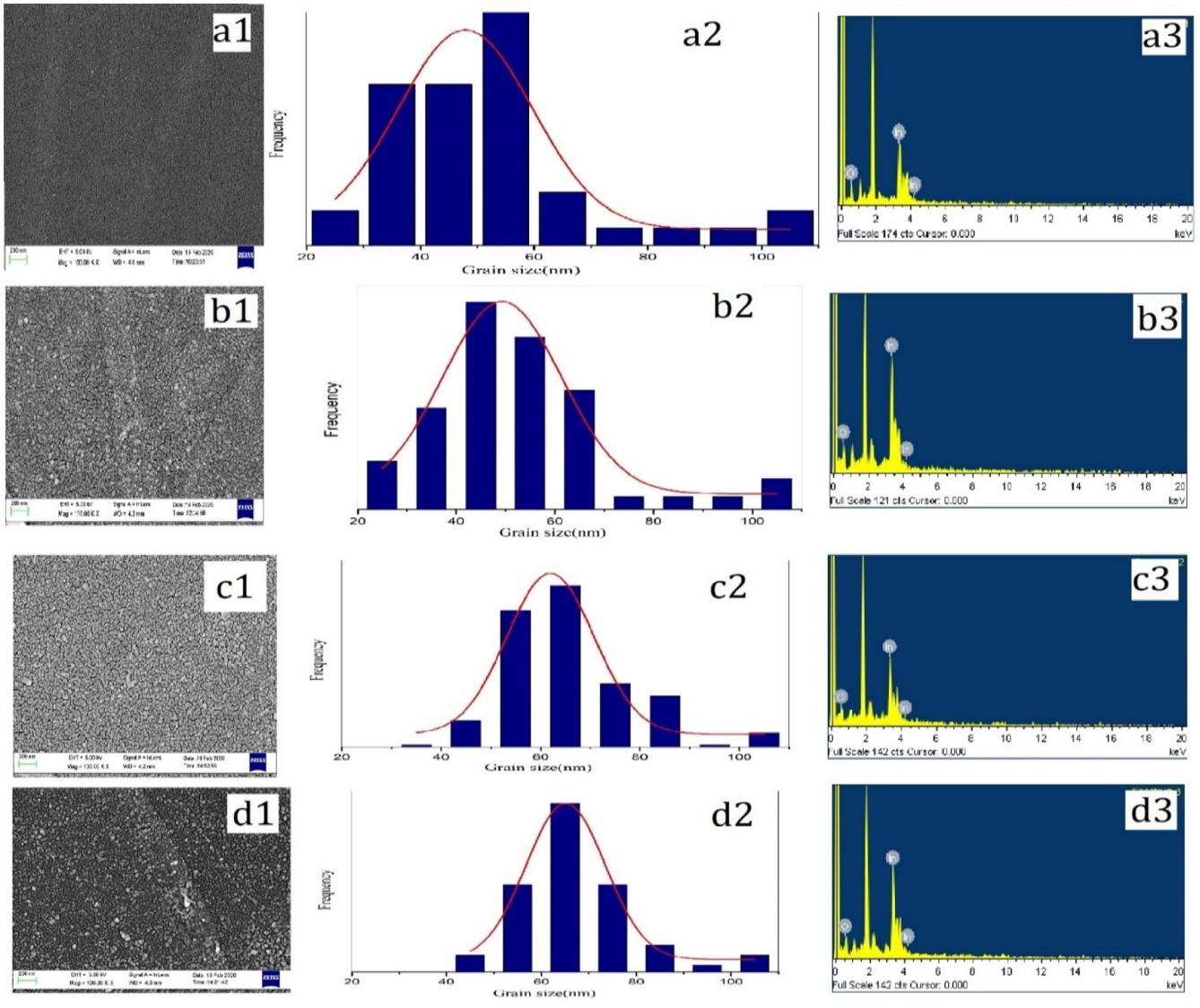


**Figure 5.** FESEM, grain size, and EDX images of $In_2O_3$ thin films sprayed at (a) 350, (b) 400, (c) 450, and (d) 500 °C.



https://doi.org/10.1021/acsomega.1c01831
*ACS Omega* 2021, 6, 17442−17454

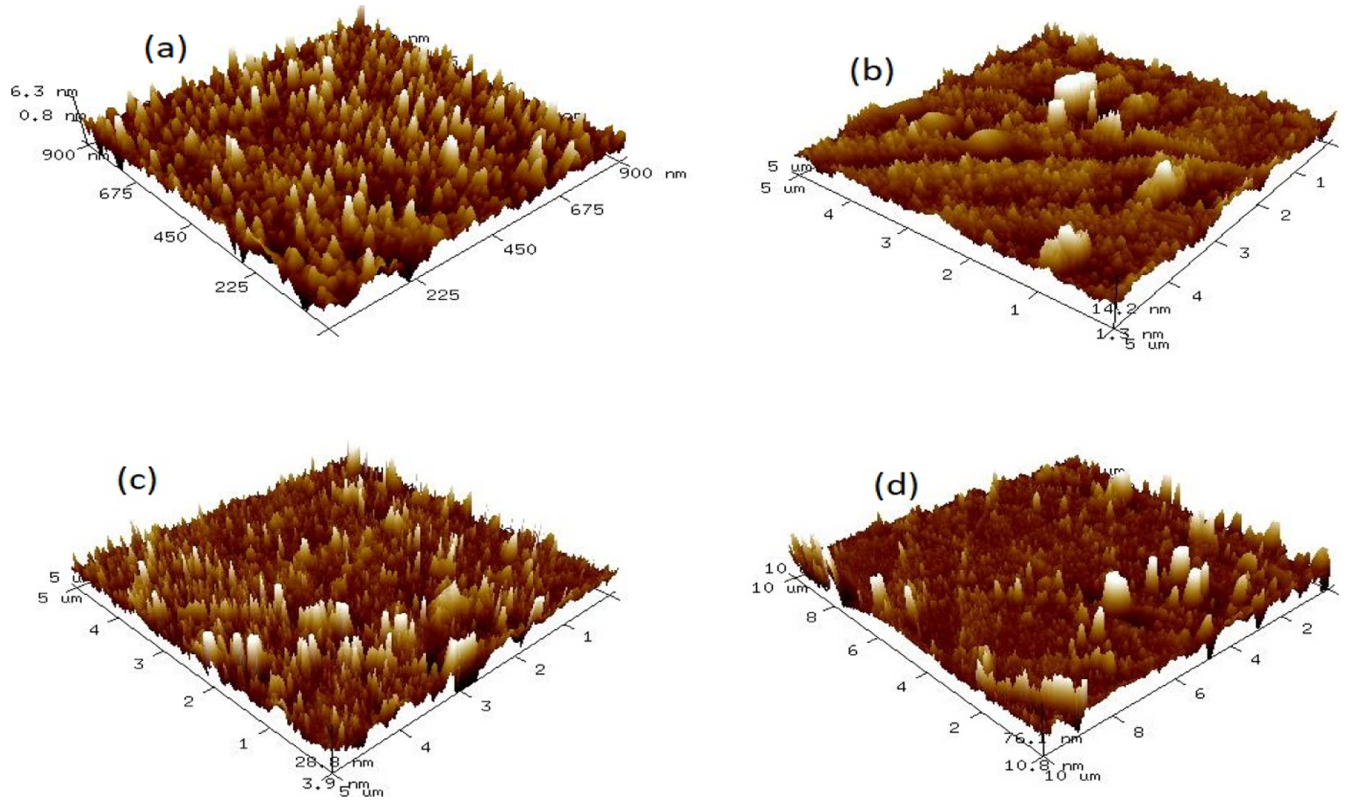


**Figure 6.** AFM images of indium oxide thin films deposited at (a) 350, (b) 400, (c) 450, and (d) 500 °C.

$$\text{Dislocation density } (\delta) = \frac{1}{(\text{crystallite size})^2} \quad (2)$$

Dislocation density is decreased with increasing substrate temperature, as the dislocation density indicates the dislocation network in the indium oxide thin films. The reduction in dislocation density reflects the emergence of good-quality thin films at higher deposition temperatures.[25] The variation of dislocation density is shown in Figure 4. The dislocation density is significantly low at high substrate temperature, leading to more carrier density and surface oxygen adsorption, which leads to enhancement of the gas-sensing properties of indium oxide thin films.

**FESEM with EDX.** The surface morphology of the thin films depends on the preparation technique and its deposition parameters. The FESEM images of indium oxide films which are sprayed at different deposition temperatures are depicted in Figure 5. All the thin films are found to be well adhered to the substrate without any pinholes. All the films possess uniform grain distribution throughout the surface of the samples. The size of the grains is enhanced with increasing substrate temperature due to the agglomeration.[26,27] The elemental analysis of thin films has been carried out using the energy-dispersive X-ray (EDX) spectrum, which validates the presence of indium and oxygen atoms only. The EDX spectra are shown in Figure 5a3−d3.

**Atomic Force Microscopy.** Atomic force microscopy (AFM) is extensively used to investigate the topographical features of the deposited indium oxide thin films at different substrate temperatures. Mainly, AFM studies assist in computing the effect of substrate temperature on the surface nature and investigating the crystal growth mechanism of the thin film. The topological properties will play an essential role in the present gas-sensing characterization. Two-dimensional images of indium oxide thin films deposited at different substrate temperatures are shown in Figure 6. The root mean square (rms) roughness of the deposited thin films is analyzed using Nanoscope E software, and it is found to decrease with increasing substrate temperature. Calculated rms roughness values are tabulated in Table 1. As substrate temperature is increasing, adatom mobility will be increased, which leads to a decrease in the surface roughness of the indium oxide thin film. Also, the film which is deposited at higher substrate temperature has perfect crystals with larger crystallite size, which will provide stronger interactions between target gas molecules and the indium thin film, in turn improving the sensitivity of the sensor element.

**Table 1. rms Roughness of Indium Oxide Films Sprayed at Various Deposition Temperatures**

| s. no. | deposition temperature (°C) | rms roughness (nm) |
|---|---|---|
| 1 | 350 | 16.8 |
| 2 | 400 | 14.3 |
| 3 | 450 | 6.04 |
| 4 | 500 | 1.33 |

**Brunauer−Emmett−Teller Surface Area Analysis.** To explain internal architectures, nitrogen adsorption−desorption investigations of the indium oxide thin film along with the corresponding pore diameter versus pore volume plot which is deposited at a substrate temperature of 500 °C are presented in Figure 7. In a mesoporous material, during the adsorption process, the molecules fill the higher energy sites which are near to the pore wall first and then lower energy sites which are away from the pore wall. When the adsorbed molecules in the


https://doi.org/10.1021/acsomega.1c01831
ACS Omega 2021, 6, 17442−17454

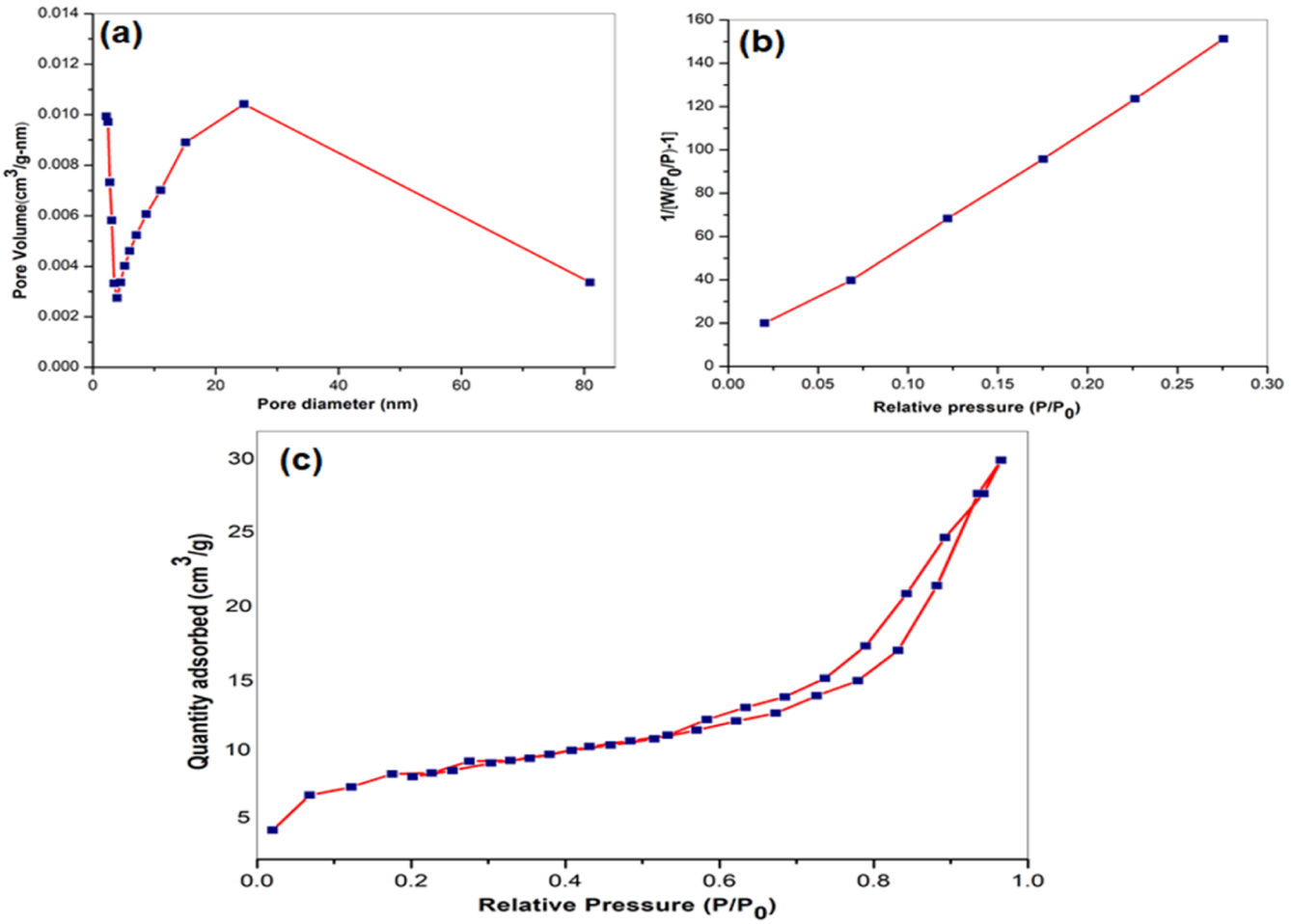


**Figure 7.** (a) BJH, (b) BET, and (c) $N_2$ adsorption−desorption isotherm of the indium oxide thin film deposited at 500 °C.

opposing walls get closer, they collapse into thermodynamically lower energy states (capillary condensation), and during the desorption process, these collapsed molecules at lower energy need higher pressure drop to get desorbed, which results in hysteresis in the adsorption and desorption isotherm.[28] Hence, it can be seen that the isotherm exhibits the IV-type mesoporous nature of the deposited indium oxide thin film. The indium oxide thin film sample's BET surface is about 37.6 $m^2/g$, which could provide large reaction sites to facilitate target gas molecules in the gas-sensing mechanism.[29,30] Pore size distribution of the sample was determined by the BJH method, and it was found to be 14.6 nm.

**Raman Spectroscopy.** Raman spectroscopy is a nondestructive advanced technique for investigating metal oxides' structural information and bringing out helpful information. Figure 8 shows the room temperature Raman spectra of indium oxide films sprayed at different temperatures. The active Raman modes are observed at a Raman shift of 558.61, 802.85, and 1097.18 $cm^{-1}$. The peak that appeared at 558.61 $cm^{-1}$ is most likely attributed to $In_2O_3$. Raman modes are observed at a Raman shift of 802.85 and 1097.18 $cm^{-1}$ and are assigned to phonons associated with the cubic-structured indium oxide thin films.[31,32] As the substrate temperature is enhanced, the full width half maxima are decreased. It is due to the reduction in the dislocation density due to a decrease in the intergranular volume fraction, which leads to increment in the size of the crystallite, which is in accordance with the XRD investigations.[32]

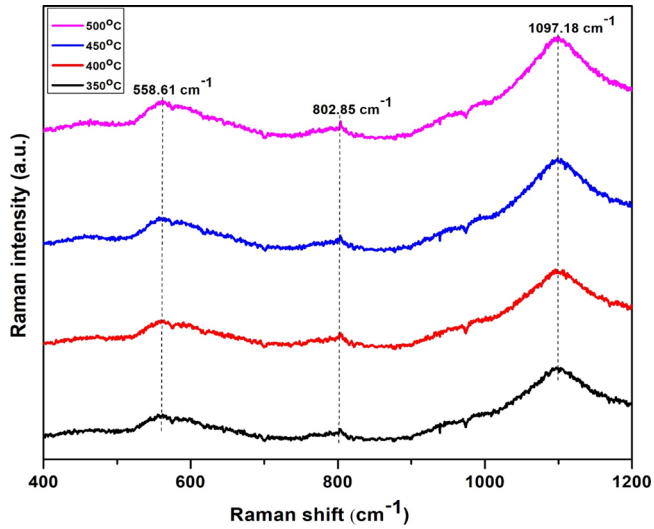


**Figure 8.** Raman spectra of $In_2O_3$ thin films.

**Photoluminescence Characterization.** Photoluminescence (PL) spectra obtained at room temperature of the indium oxide thin film deposited at 500 °C are investigated using a xenon source with an excitation wavelength of 280 nm, as depicted in Figure 9. The standard indium oxide has a strong and broad emission peak near 330 nm. The peak near 387 nm is evoked owing to the exciton recombination process,


https://doi.org/10.1021/acsomega.1c01831
ACS Omega 2021, 6, 17442−17454

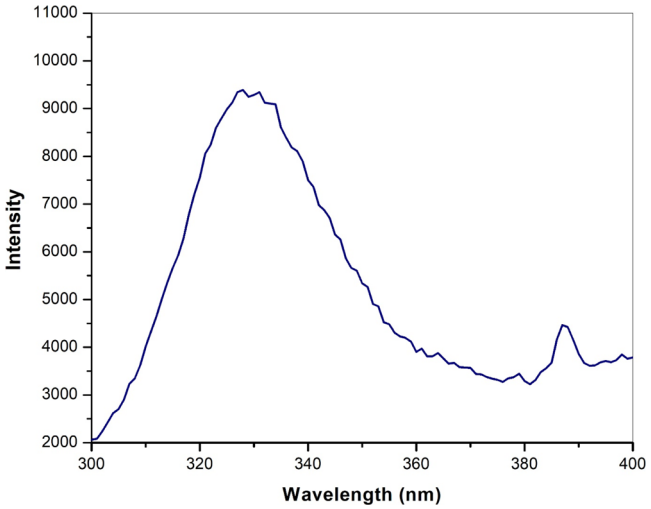


**Figure 9.** PL spectra of the indium oxide thin film deposited at 500 °C.

which plays a vital role in influencing the optical emission.[33,34] The emission at this wavelength might be due to the oxygen vacancies existing in the sample. The formation of oxygen vacancies in the deposited nanostructured $In_2O_3$ thin films can be described as follows. At the time of deposition, a few oxygen sites evolve into oxygen-deficient sites, or maybe, several intrinsic imperfections appear, which leads to the creation of oxygen vacancies. The crackdown of defect-related emission of indium oxide is related to the reconstruction of imperfect nanostructures. These generated oxygen vacancies will create a new energy level close to or within the indium oxide thin films' energy band gap, which might generally be acting as deep defect donor levels. The ultraviolet emission of the indium oxide thin films could be the radiative recombination process of the electrons and photoexcited holes absorbed by oxygen vacancies.[35]

**Transmission Electron Microscopy.** To understand the microstructure of the films, transmission electron microscopy (TEM) is carried out in detail. Figure 10a shows the TEM images of the indium oxide thin film deposited at a substrate temperature of 500 °C. Figure 10b depicts the selected area electron diffraction (SAED) pattern. It shows a set of diffraction rings, which indicates the polycrystalline nature of the prepared indium oxide thin films. The characteristic planes (211), (222), (431), and (400) correspond to the simple cubic structure of indium oxide, which is in agreement with XRD studies.

The lattice spacing ($d$) might be determined using the following formula[36]

$$\text{lattice spacing } (d) = \frac{L\lambda}{R} \tag{3}$$

where "$\lambda$" is the electron wavelength (0.0027 nm), $L$ is the length of the camera (100 mm), and $R$ is the radius of the concentric ring, which is estimated from the central bright spot. The calculated lattice spacing ($d$) values using the abovementioned eq 3 are good in agreement with the (222) orientation of the XRD studies.

**Optical Properties.** The optical properties of indium oxide thin films strongly depend on the microstructure, film thickness, and deposition parameters. Figure 11 shows the absorption spectra of indium oxide films sprayed at different deposition temperatures. Figure 12 depicts the transmittance spectra of indium oxide thin films prepared at various substrate temperatures. The average transmittance of the indium oxide films is more than 72% in the visible region. The transmittance is found to rise by enhancing the deposition temperature. It may be owing to the increased carrier concentration because of oxygen deficiency.[11]

The optical band gap ($E_g$) of indium oxide thin films sprayed at various substrate temperatures is determined by adopting the Tauc expression using the absorption spectra.[37]

$$\alpha h\nu = B(h\nu - E_g)^x \tag{4}$$

Tauc plots of indium oxide films are depicted in Figure 13. The optical band gap ($E_g$) will be determined by estimating the linear segment of the absorption line to the horizontal axis. Estimated optical energy band gaps of indium oxide thin films sprayed at various deposition temperatures are tabulated in Table 2. The optical band gap is decreased with increasing substrate temperature, and it is due to the quantum confinement effect when the particle size is in the nanoscale.

**Gas-Sensing Measurements.** *Sensitivity and Selectivity.* The room temperature sensitivity of the indium oxide films, which are sprayed at different substrate temperatures toward 50 ppm toluene, is determined using eq 1. In comparison with toluene, several other gases such as methanol, ethanol, acetone, *n*-butanol, and benzene are tested at a concentration of 50 ppm toward different types of sensor elements sprayed at various substrate temperatures. The selectivity characteristics of indium oxide thin film sensors toward other gases are depicted

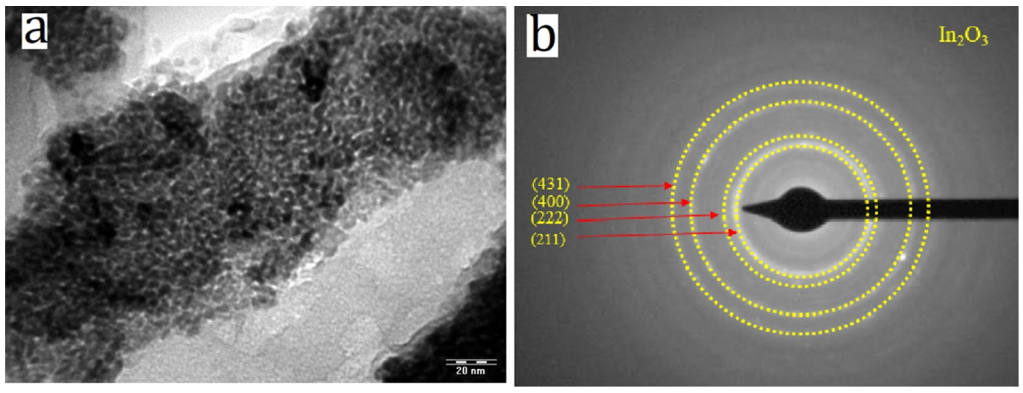


**Figure 10.** TEM images of the $In_2O_3$ thin film deposited at 500 °C (a). (b) SAED of the $In_2O_3$ thin film deposited at 500 °C.


https://doi.org/10.1021/acsomega.1c01831
ACS Omega 2021, 6, 17442−17454

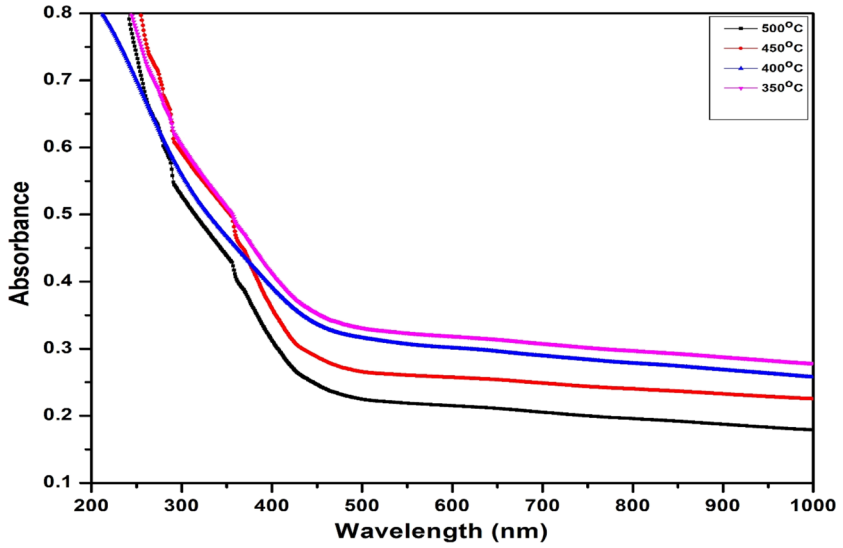


**Figure 11.** Absorption spectra of indium oxide thin films.

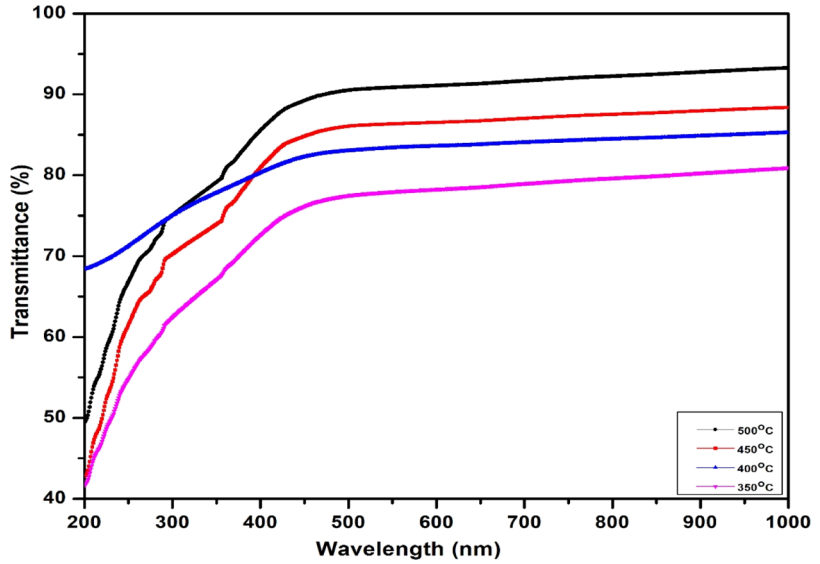


**Figure 12.** Transmittance spectra of indium oxide films.

in Figure 14. Thus, it is concluded that the sensor element, which is sprayed at a substrate temperature of 500 °C, has shown outstanding selectivity and sensitivity toward toluene at room temperature. It is well known that the gas-sensing mechanism in oxide-based materials is surface-controlled, and each chemical reaction depends on the activation energy of the material. An increase in film sensitivity with an increase in substrate temperature may be due to the decrease in activation energy at increased substrate temperature. Thus, a relatively higher sensitivity has been observed for the sample which is deposited at 500 °C.[38] Also, toluene has shown the best selectivity due to its lower dissociation energy in comparison with that of other vapors. Due to the lower dissociation energy, bonds in toluene can be easily broken to behave with the sensing element; subsequently, a considerable number of free electrons are liberated at the time of the reaction, which causes enough change in the resistance of the sensor, affecting the high sensitivity toward toluene.[39] Dong et al.[40] reported hierarchical rosette-like $In_2O_3$ microsphere- and hollow microsphere-based sensors to detect toluene vapors at an operating temperature of 350 °C. Xiao et al.[41] synthesized indium oxide nanotubes using an electrospinning method for toluene-sensing properties at an optimum operating temperature of 340 °C toward 100 ppm. Xu et al.[42] investigated gas-sensing properties of hexagonal indium oxide nanorods prepared by a solvothermal method. They reported that indium oxide nanorods are sensitive toward different vapors at an operating temperature of 330 °C. Their sensor element has shown a response of 1.8 toward 500 ppm toluene. To the best of our knowledge and belief, majority of the indium oxide-based sensors are operated relatively at high operating temperatures to trace high concentrations of toluene vapors. Hence, our indium oxide thin film sensor, which is deposited with a cost-effective spray pyrolysis technique, is further utilized to study other gas-sensing characterizations such as stability, repeatability, and dynamic response.

*Stability and Repeatability.* The long-term stability and repeatability of a sensor element will play an essential role in real-time gas sensor applications. The long-term stability of the indium oxide sensor deposited at 500 °C has been reported


https://doi.org/10.1021/acsomega.1c01831
ACS Omega 2021, 6, 17442−17454

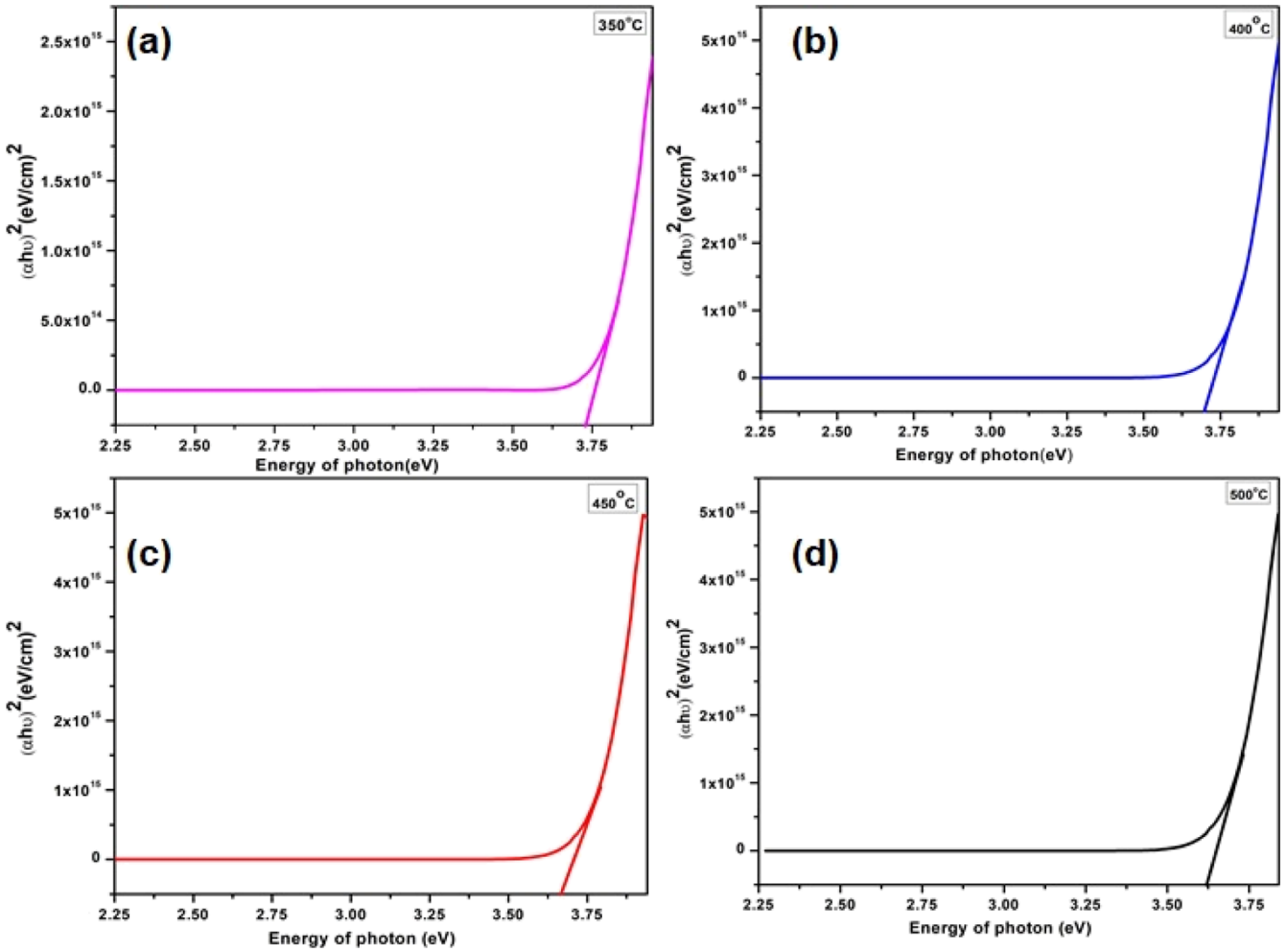


**Figure 13.** Tauc plot of the indium oxide thin films deposited at (a) 350, (b) 400, (c) 450, and (d) 500 °C.

**Table 2. Optical Band Gap of Indium Oxide Films**

| s. no. | deposition temperature (°C) | optical band gap (eV) |
|---|---|---|
| 1 | 350 | 3.72 |
| 2 | 400 | 3.69 |
| 3 | 450 | 3.67 |
| 4 | 500 | 3.62 |

over a period of 30 days, as depicted in Figure 15. The sensor element has shown almost a stable response value during the period, as mentioned earlier, which indicates that the sensor has good stability. To investigate the repeatability, the gas-sensing test has been carried out continuously for four cycles toward 50 ppm toluene at room temperature, as shown in Figure 16; the response values have shown a negligible variation during the repeated cycles. Hence, we can conclude that the fabricated sensor has excellent repeatability property.

*Transient Response Characteristics of the Sensor.* The response−recovery studies investigate essential parameters in real-time application to detect harmful gases. The transient response toward 50 ppm toluene is studied at room temperature, as depicted in Figure 17. As noticed from the results, the indium oxide sensor deposited at 500 °C shows a classical n-type sensing behavior with large resistance in the presence of air, and the resistance of the sensor drops down when exposed to a reducing test gas (toluene). From the figure, it is clear that recovery and response times are 26 and 28 s, respectively. Comparison of toluene-sensing properties of different metal oxides available in the literature along with the present work is tabulated in Table 3.

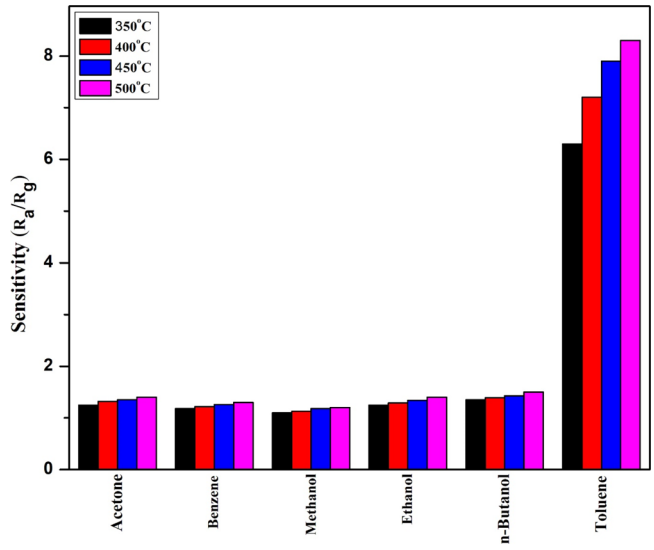


**Figure 14.** Response of $In_2O_3$ thin films deposited at different substrate temperatures (350, 400, 450, and 500 °C) toward 50 ppm of various gases at room temperature.


https://doi.org/10.1021/acsomega.1c01831
ACS Omega 2021, 6, 17442−17454

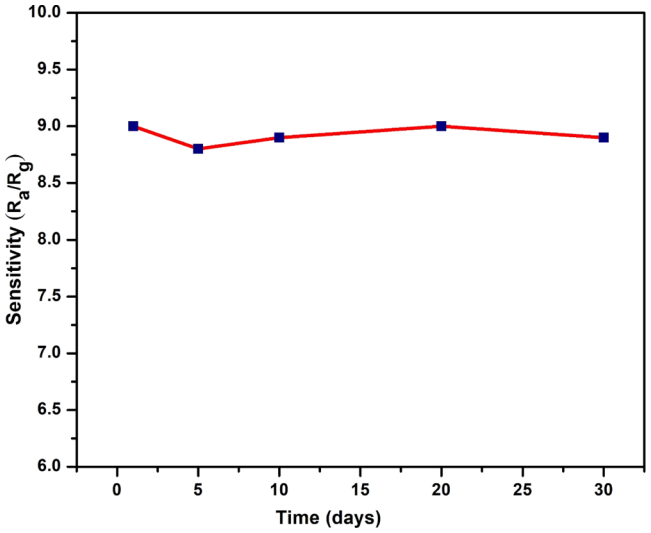


**Figure 15.** Long-term stability of the pure $In_2O_3$ gas sensor deposited at 500 °C toward 50 ppm toluene at room temperature.

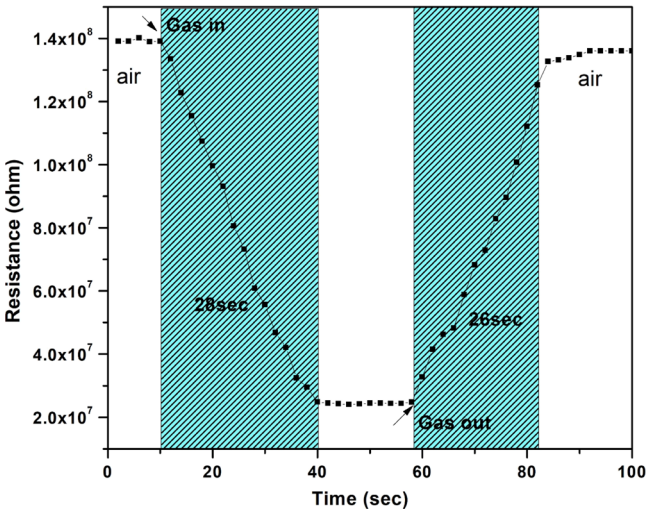


**Figure 17.** Transient response curves of indium oxide thin films which are deposited at 500 °C.

## CONCLUSIONS

Indium oxide thin films are prepared using a cost-effective chemical spray pyrolysis technique. The effects of substrate temperature on microstructural, morphological, optical, and gas-sensing characteristics are systematically investigated. Crystallite size is increased and dislocation density is reduced with increasing deposition temperature. The nanostructured nature of the deposited thin film is confirmed using TEM. Atomic force microscopy studies revealed that the thin film sprayed at a deposition temperature of 500 °C exhibited the least rms roughness. The band gap of films is determined using the Tauc plot, and it is decreased with increasing substrate temperature. Gas-sensing characterization of indium oxide films is studied toward various volatile organic compounds such as acetone, methanol, ethanol, benzene, *n*-butanol, and toluene at room temperature. The film, which is sprayed at 500 °C, has exhibited the best sensitivity toward toluene at room temperature. It is also observed that the $In_2O_3$ thin film has shown excellent stability and repeatability with response and recovery times of 28 and 26 s, respectively.

## EXPERIMENTAL DETAILS

**Materials and Thin-Film Preparation.** Analytical-grade indium acetate (99.9% pure) was purchased from Sigma-Aldrich (India), and it is used as a starting precursor without further purification. The required amount of indium acetate was dissolved in deionized water and stirred on a magnetic stirrer for 30 min at room temperature. After 10 min, few drops of acetic acid were added to the abovementioned solution to obtain a clear solution. The glass substrates (Blue Star-India with a thickness of 1 mm) are cleaned with particle-free solution, then followed by ultrasonication in acetone and ethanol for 20 min, and cleaned with double-distilled water and heated at 100 °C using a programmable furnace for 30 min and dried in a hot air oven. The obtained solution is filled into a 50 mL quartz spray container. The solution is deposited with a computer-interfaced spray pyrolysis system at different substrate (deposition) temperatures ranging from 350 to 500 °C with a flow rate of 1 mL/min and deposited for 10 min. The nozzle-to-substrate distance was maintained at 25 cm, and filtered compressed air has been used as a carrier gas at a

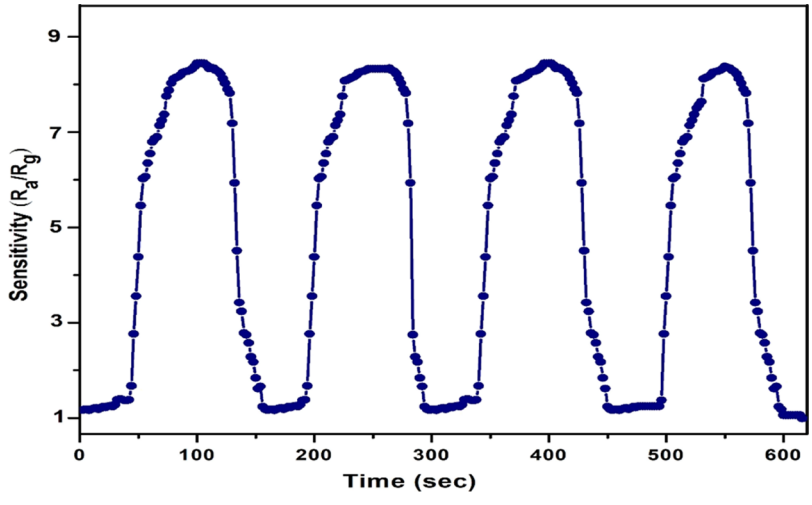


**Figure 16.** Repeatability of indium oxide thin films sprayed at 500 °C toward 50 ppm toluene.



https://doi.org/10.1021/acsomega.1c01831
*ACS Omega* 2021, 6, 17442−17454

**Table 3. Comparison of Toluene-Sensing Properties of Different Metal Oxides Available in the Literature along with the Present Work**

| gas-sensing materials | toluene concentration (ppm) | operating temperature (°C) | response/recovery times | reference |
|---|---|---|---|---|
| Au/ZnO NPs | 100 ppm | 377 | 20 min/6 min | 43 |
| clustering $SnO_2$ NPs | 50 ppm | 250 | | 44 |
| CdS−$TiO_2$ | 5000 ppm | 27 | 70 s/125 s | 45 |
| Ce−$SnO_2$ coral-like | 50 ppm | 190 | | 46 |
| Pt NP-decorated $In_2O_3$ NFs | 10 ppm | 250 | | 47 |
| Au−ZnO NWs | 500 ppm | 340 | 32 s/57 s | 48 |
| $SnO_2$ NFs | 1−300 ppm | 350 | 1 s/5 s | 49 |
| $TiO_2$−ZnO Nanoflowers | 100 ppm | 290 | | 50 |
| MWCNT/$SnO_2$ NCs | 1000 ppm | 250 | 24 s/14 s | 51 |
| C-$WO_3$ | 1000 ppb | 320 | 40 s/10 s | 52 |
| Au/ZnO nanoparticles | 100 ppm | 377 | NA/300 s | 53 |
| $Co_3O_4$ nanorods | | 200 | 90/55 | 54 |
| pure $In_2O_3$ | 50 ppm | 27 | 28 s/26 s | present work |

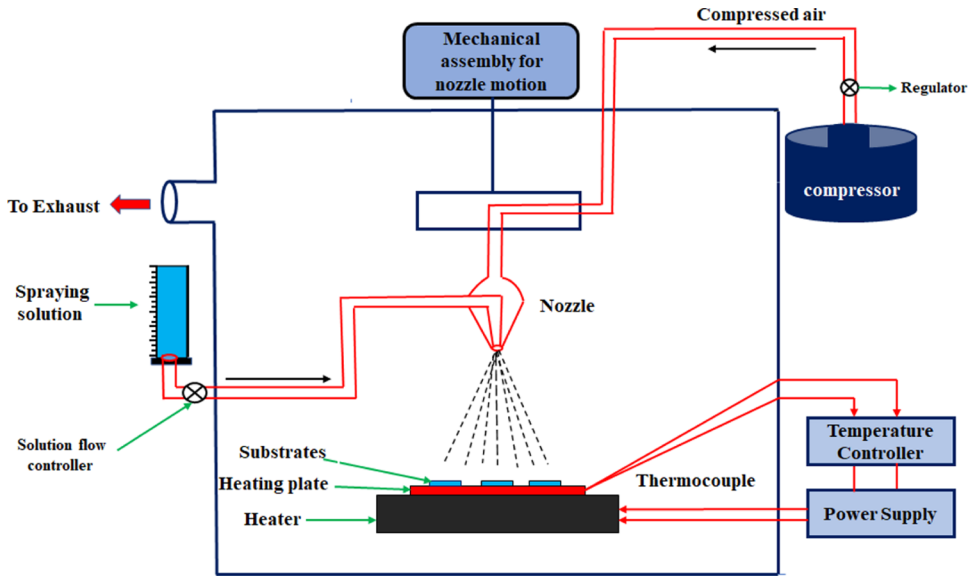


**Figure 18.** Schematic diagram of spray pyrolysis equipment.

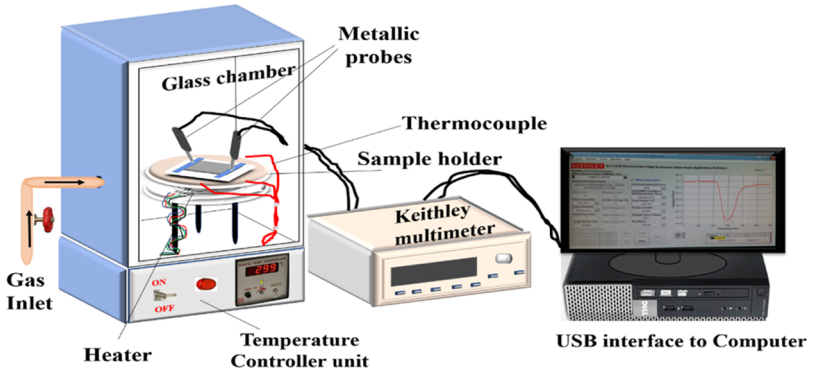


**Figure 19.** Schematic diagram of the gas-sensing system.

pressure of 1 bar. A schematic diagram of the spray pyrolysis system is depicted in Figure 18.

**Material Characterization.** Thin-film thickness was determined using a stylus profiler (SJ-301 Mitutoyo Surface Profilometer). The structural characterization and crystallinity of the indium oxide thin films sprayed at various substrate temperatures were investigated using a Bruker X-ray diffractometer (Bruker D8) with Cu K$\alpha$ as a radiation source (0.154 nm) in the grazing incident mode with a rate of scanning 2°/min. The morphology of the indium oxide thin films has been investigated by FESEM (Carl ZEISS EVO-18, Germany), and elemental analysis of thin films was carried out using EDX. The surface roughness of the indium oxide films has been determined by AFM (Innova, Bruker). The indium oxide thin films' optical properties and energy band gap were investigated using a UV−Vis spectrophotometer (Analytical


https://doi.org/10.1021/acsomega.1c01831
ACS Omega 2021, 6, 17442−17454

jena, specord 210 Plus) in the spectral range of 400−800 nm. The variation in crystal defects of indium oxide thin films was investigated using Raman spectroscopy (Labram-HR800). PL spectra have been obtained using the HORIBA Fluorolog 3. TEM was carried out to explain the nanostructure of the thin films using the TECNAI 20G2 operating at 200 kV. The TEM investigations were performed in both the image and diffraction modes.

**Fabrication of the Thin-Film Gas Sensor.** To study the gas-sensing characterization of deposited indium oxide thin films, Ohmic contacts were made on both ends of the film with silver paste and copper wires. These sensor elements were sintered for 2 h at 150 °C to ensure good contact of electrodes. They were utilized to study the gas-sensing characteristics of different gases such as ethanol, acetone formaldehyde, ammonia, methanol, and toluene with a concentration of 50 ppm at room temperature. A schematic figure of the gas-sensing system is depicted in Figure 19. Humidity will decrease the stability of the sensor; hence, we have maintained the relative humidity in the chamber at 60% with the help of a digital humidity controller (Humitherm, India) during the gas-sensing measurements.[55,56]

$$\text{Sensitivity } (S) = \frac{R_a}{R_g} \tag{5}$$

where $R_g$ = resistance of the sensor in the presence of target gas and $R_a$ = resistance of the sensor in the presence of air.

## AUTHOR INFORMATION


### Corresponding Author

**Pothukanuri Nagaraju** − *Nanosensor Research Laboratory, Department of Physics, CMR Technical Campus, Hyderabad, Telangana State 501 401, India;* orcid.org/0000-0003-1894-6825; Email: nagarajuphysics@gmail.com

### Authors

**Sunil Gavaskar Dasari** − *Thin Films & Nanomaterials Research Laboratory, Department of Physics, Osmania University, Hyderabad, Telangana State 500 007, India*

**Vijayakumar Yelsani** − *Department of Physics, Anurag University, Hyderabad, Telangana State 500 088, India*

**Sreekanth Tirumala** − *Department of Physics, JNTUH College of Engineering Jagtial, Nachupally (Kondagattu), Telangana State 505 501, India*

**Ramana Reddy M V** − *Thin Films & Nanomaterials Research Laboratory, Department of Physics, Osmania University, Hyderabad, Telangana State 500 007, India*

Complete contact information is available at: https://pubs.acs.org/10.1021/acsomega.1c01831


### Notes

The authors declare no competing financial interest.

## ACKNOWLEDGMENTS

The authors thank the Head, Department of Physics, Osmania University, Hyderabad for providing necessary experimental facilities to carryout this work. DSG thankful to UGC-New Delhi, India for providing fincancial assistance in the form of NET-JRF during the tenure of this work. R.R.M.V. sincerely thanks science and engineering research board, New Delhi, for providing the necessary financial support under a research project with the file number (file no.: EMR/2017/002651) to carry out the present work. P.N. wishes to acknowledge the JNTU-Hyderabad for supporting the current work with reference number JNTUH/TEQIP-III/CRS/2019/Physics 01, and V.Y. wishes to acknowledge the JNTU-Hyderabad for funding the present work with reference number JNTUH/TEQIP-III/CRS/2019/Physics 03. The authors also thank the UGC-NRC, School of Physics, University of Hyderabad for providing FESEM facility. The authors would like express their sincere grattitude to Dr. N. P. Lalla, Scientist-H, Dr. Vasant Sathe, Scientist-H, UGC-DAE-CSR, Indore, for providing experimental facilities in their laboratories. The authors also express their sincere grattitude to Dr. P. S. Reddy, NIT-Goa, for providing AFM measurments.

## REFERENCES


(1) Williams, D. E. Semiconducting oxides as gas-sensitive resistors. *Sens. Actuators, B* **1999**, *57*, 1−16.

(2) Li, C.; Zhang, D.; Liu, X.; Han, S.; Tang, T.; Han, J.; Zhou, C. $In_2O_3$ nanowires as chemical sensors. *Appl. Phys. Lett.* **2003**, *82*, 1613−1615.

(3) Soulantica, K.; Erades, L.; Sauvan, M.; et al. Synthesis of indium and indium oxidenanoparticles from indium cyclopentadienyl precursor and their application for gas sensing. *Adv. Funct. Mater.* **2003**, *13*, 553−557.

(4) Li, X.; Yao, S.; Liu, J.; Sun, P.; Sun, Y.; Gao, Y.; Lu, G. Vitamin C-assisted synthesisand gas sensing properties of coaxial In $_2O_3$ nanorod bundles. *Sens. Actuators, B* **2015**, *220*, 68−74.

(5) Koundourakis, G.; Rockstuhl, C.; Papazoglou, D.; Klini, A.; Zergioti, I.; Vainos, N. A.; Fotakis, C. Laser printing of active optical microstructures. *Appl. Phys. Lett.* **2001**, *78*, 868−870.

(6) Babu, P. M.; Radhakrishnaa, B.; Venkata Rao, G.; Sreedhara Reddy, P.; Uthanna, S. *J. Optoelectron. Adv. Mater.* **2004**, *6*, 205−210.

(7) Gîrtan, M.; Rusu, G. On the Size Effect in $In_2O_3$ Thin Films. *Mater. Sci. Eng., B* **1999**, *XLV−XLVI*, 166−172.

(8) Mailis, S.; Boutsikaris, L.; Vainos, N. A.; Xirouhaki, C.; Vasiliou, G.; Garawal, N.; Kiriakidis, G.; Fritzsche, H. Holographic recording in indium−oxide ($In_2O_3$) and indium−tin−oxide ($In_2O_3$:Sn) thin films. *Appl. Phys. Lett.* **1996**, *69*, 2459−2461.

(9) Veeraswamy, Y.; Sunil Gavaskar, D.; Choudhary, R. J.; Phase, D. M.; Ramana Reddy, M. V. Structural and photoluminescence properties of Ta: $In_2O_3$ thin films grown by pulsed laser deposition technique. *AIP Conf. Proc.* **2018**, *2005*, 060003.

(10) Senthilkumar, V.; Vickraman, P. Annealing temperature dependent on structural, optical and electrical properties of indium oxide thin films deposited by electron beam evaporation method. *Curr. Appl. Phys.* **2010**, *10*, 880−885.

(11) Xu, J.; Yang, Z.; Zhang, X.; Yang, L.; Xu, H.; Wang, H. Study on Needles and Cracks of Tin-doped Indium Oxide Tablets for Electron Beam Evaporation Process. *Mater. Res.* **2015**, *18*, 519−524.

(12) Chung, W.-Y. Gas-sensing properties of spin coted indium oxide film on various substrates. *J. Mater. Sci.: Mater. Elec.* **2001**, *12*, 591−596.

(13) Sunde, T. O. L.; Garskaite, E.; Otter, B.; Fossheim, H. E.; Sæterli, R.; Holmestad, R.; Einarsrud, M.-A.; Grande, T. Transparent and conducting ITO thin films by spin coating of an aqueous precursor solution. *J. Mater. Chem.* **2012**, *22*, 15740−15749.

(14) Ramanathan, G.; Murali, K. R. Dip Coated Indium Oxide Films and Their Optical Constants. *Trans. Electr. Electron. Mater.* **2020**, *21*, 513−518.

(15) Seki, Y.; Sawada, Y.; Wang, M. H.; Lei, H.; Hoshi, Y.; Uchida, T. Electrical properties of tin-doped indium oxide thin films prepared by a dip coating. *Ceram. Int.* **2012**, *38*, S613−S616.

(16) Pramod, N. G.; Pandey, S. N.; Sahay, P. P. Sn-Doped In2O3 Nanocrystalline Thin Films Deposited by Spray Pyrolysis: Microstructural, Optical, Electrical, and Formaldehyde-Sensing Characteristics. *J. Therm. Spray Technol.* **2013**, *22*, 1035−1043.

(17) Qiao, L.; Bing, Y.; Wang, Y.; Yu, S.; Liang, Z.; Zeng, Y. Enhanced toluene sensing performances of Pd- loaded $SnO_2$ cubic nanocages with porous nanoparticle-assembled shells. *Sens. Actuators, B* **2017**, *241*, 1121−1129.
(18) Xu, F.; Guo, S.; Luo, Y.-L. Novel THTBN/MWNTs-OH polyurethane conducting composite thin films for applications in detection of volatile organic compounds. *Mater. Chem. Phys.* **2014**, *145*, 222−231.
(19) Nagaraju, P.; Vijayakumar, Y.; Reddy, M. V. R.; Deshpande, U. P. Effect of vanadium pentoxide concentration in $ZnO/V_2O_5$ nanostructured composite thin films for toluene detection. *RSC Adv.* **2019**, *9*, 16515−16524.
(20) Kou, L.; Zhang, D.; Liu, D. A Novel Medical E-Nose Signal Analysis System. *Sensors* **2017**, *17*, 402.
(21) Nagaraju, P.; Vijayakumar, Y.; Reddy, G. L. N.; Ramana Reddy, M. V. ZnO wrinkled nanostructures: enhanced BTX sensing. *J. Mater. Sci.: Mater. Electron.* **2018**, *29*, 11457−11465.
(22) Nagaraju, P.; Vijayakumar, Y.; Phase, D. M.; Choudary, R. J.; Ramana Reddy, M. V. Microstructural, optical and gas sensing characterisation of laser ablated nanostructured ceria thin films. *J. Mater. Sci.: Mater. Electron.* **2016**, *27*, 651−658.
(23) Nagaraju, P.; VijayaKumar, Y.; Radhika, P.; Choudhary, R. J.; RamanaReddy, M. V. Structural, morphological, optical and gas sensing properties of nanocrystalline ceria thin films. *Mater. Today: Proc.* **2016**, *3*, 4009−4018.
(24) Nagaraju, P.; VijayaKumar, Y.; Phase, D.; Reddy, V.; Ramana Reddy, M. Preparation and microstructural characterisation of Si(100) $Ce_{1-x}Gd_xO_{2-\delta}$ thin films prepared by pulsed laser deposition technique. *Mater. Sci.* **2014**, *32*, 541−546.
(25) Nagaraju, P.; Vijayakumar, Y.; Choudhary, R. J.; Ramana Reddy, M. V. Preparation and characterisation of nanostructured Gd doped cerium oxide thin films by pulsed laser deposition for acetone sensor application. *Mater. Sci. Eng., B* **2017**, *226*, 99−106.
(26) Zhang, L.; Lan, J.; Yang, J.; Guo, S.; Peng, J.; Zhang, L.; Tian, S.; Ju, S.; Xie, W. Study on the physical properties of indium tin oxide thin films deposited by microwave-assisted spray pyrolysis. *J. Alloys Compd.* **2017**, *728*, 1338−1345.
(27) Heo, K. C.; Son, P. K.; Sohn, Y.; Yi, J.; Kwon, J. H.; Gwag, J. S. Characteristics of Ion Beam Assisted ITO Thin Films Deposited by RF Magnetron Sputtering. *Mol. Cryst. Liq. Cryst.* **2014**, *601*, 57−63.
(28) Gondal, M. A.; Dastageer, M. A.; Oloore, L. E.; Baig, U.; Rashid, S. G. Enhanced photo-catalytic activity of ordered mesoporous indium oxide nanocrystals in the conversion of $CO_2$ into methanol. *J. Environ. Sci. Health* **2017**, *52*, 785−793.
(29) Wang, Z.; Hou, C.; De, Q.; Gu, F.; Han, D. One-step Synthesis of Co-doped $In_2O_3$ Nanorods for High Response of Formaldehyde Sensor at Low Temperature. *ACS Sens.* **2018**, *3*, 468−475.
(30) Zhang, X.; Song, D.; Liu, Q.; Chen, R.; Hou, J.; Liu, J.; Zhang, H.; Yu, J.; Liu, P.; Wang, J. Designed synthesis of Ag-functionalised Ni-doped $In_2O_3$ nanorods with enhanced formaldehyde gas sensing properties. *J. Mater. Chem. C* **2019**, *7*, 7219−7229.
(31) Gwamuri, J.; Marikkannan, M.; Mayandi, J.; Bowen, P.; Pearce, J. Influence of Oxygen Concentration on the Performance of Ultra-Thin RF Magnetron Sputter Deposited Indium Tin Oxide Films as a Top Electrode for Photovoltaic Devices. *Materials* **2016**, *9*, 63.
(32) Chandrasekhar, R.; Choy, K. L. Innovative and cost-effective synthesis of indium tin oxide films. *Thin Solid Films* **2001**, *398−399*, 59.
(33) Gu, F.; Wang, S. F.; Lü, M. K.; Zhou, G. J.; Xu, D.; Yuan, D. R. Photoluminescence Properties of $SnO_2$ Nanoparticles Synthesised by Sol−Gel Method. *J. Phys. Chem. B* **2004**, *108*, 8119−8123.
(34) Narmada, A.; Kathirvel, P.; Mohan, L.; Saravanakumar, S.; Marnadu, R.; Chandrasekaran, J. Jet Nebuliser sray pyrolysed Indium Oxide and Nickel doped Indium Oxide thin films for photodiode application. *Optik* **2020**, *202*, 163701.
(35) Ullah, H.; Yamani, Z. H.; Qurashi, A.; Iqbal, J.; Safeen, K. Study of the optical and gas sensing properties of $In_2O_3$ nanoparticles synthesised by rapid sonochemical method. *J. Mater. Sci.: Mater. Electron.* **2020**, *31*, 17474−17481.
(36) Vijayakumar, Y.; Nagaraju, P.; Yaragani, V.; Parne, S. R.; Awwad, N. S.; Ramana Reddy, M. V. Nanostructured Al and Fe co-doped ZnO thin films for enhanced ammonia detection. *Phys. B* **2020**, *581*, 411976.
(37) Bhat, P.; Naveen Kumar, S. K.; Nagaraju, P. Fabrication of ultrasensitive hexagonal disc structured ZnO thin film sensor to trace nitric oxide. *J. Asian Ceram. Soc.* **2021**, *9*, 96.
(38) Shewale, P. S.; Kamble, B. N.; Moholkar, A. V.; Kim, J. H.; Uplane, M. D. Influence of Substrate Temperature on $H_2S$ Gas Sensing Properties of Nanocrystalline Zinc Oxide Thin Films Prepared by Advanced Spray Pyrolysis. *IEEE Sens. J.* **2013**, *13*, 1992−1998.
(39) Wang, L.; Li, Y.; Yue, W.; Gao, S.; Zhang, C.; Chen, Z. High-Performance Formaldehyde Gas Sensor Based on Cu-doped $Sn_3O_4$ Hierarchical Nanoflowers. *IEEE Sens. J.* **2020**, *20*, 6945−6953.
(40) Dong, H.; Liu, Y.; Li, G.; Wang, X.; Xu, D.; Chen, Z.; Zhang, T.; Wang, J.; Zhang, L. Hierarchically rosette-like In2O3 micro-spheres for volatile organic compounds gas sensors. *Sens. Actuators, B* **2013**, *178*, 302−309.
(41) Chi, X.; Liu, C.; Zhang, J.; Liu, L.; Li, H.; He, Y.; Bo, X.; Liu, L. Toluene-sensing properties of $In_2O_3$ nanotubes synthesized by electrospinning. *J. Semicond.* **2014**, *35*, 064005.
(42) Xu, J.; Chen, Y.; Shen, J. Ethanol sensor based on hexagonal indium oxide nanorods prepared by solvothermal methods. *Mater. Lett.* **2008**, *62*, 1363−1365.
(43) Suematsu, K.; Watanabe, K.; Tou, A.; Sun, Y.; Shimanoe, K. Ultraselective Toluene Gas Sensor: Nanosized Gold Loaded on Zinc Oxide Nanoparticles. *Anal. Chem.* **2018**, *90*, 1959−1966.
(44) Suematsu, K.; Shin, Y.; Hua, Z.; Yoshida, K.; Yuasa, M.; Kida, T.; Shimanoe, K. Nanoparticle Cluster Gas Sensor: Controlled Clustering of $SnO_2$ Nanoparticles for Highly Sensitive Toluene Detection. *ACS Appl. Mater. Interfaces* **2014**, *6*, 5319−5326.
(45) Partridge, M.; Wong, R.; James, S. W.; Davis, F.; Higson, S. P. J.; Tatam, R. P. Long period grating based toluene sensor for use with water contamination. *Sens. Actuators, B* **2014**, *203*, 621−625.
(46) Qu, Y.; Wang, H.; Chen, H.; xiao, J.; Lin, Z.; Dai, K. Highly sensitive and selective toluene sensor of Ce-doped coral-like $SnO_2$. *RSC Adv.* **2015**, *5*, 16446−16449.
(47) Im, D.; Park, K.-B.; Kang, J.-G.; Park, J.-S.; Kwak, S.-M.; Kwon, S.-H.; Chun, M.; Jung, H. Toluene Gas Sensing Properties of Pt-Nanoparticle-Decorated Indium Oxide Nanofibers on a Low-Power Consumable Bridge-Type Micro-Platform. *J. Korean Phys. Soc.* **2019**, *74*, 600−606.
(48) Wang, L.; Wang, S.; Xu, M.; Hu, X.; Zhang, H.; Wang, Y.; Huang, W. A Au-functionalized ZnO nanowire gas sensor for detection of benzene and toluene. *Phys. Chem. Chem. Phys.* **2013**, *15*, 17179−17186.
(49) Qi, Q.; Zhang, T.; Liu, L.; Zheng, X. Synthesis and toluene sensing properties of $SnO_2$ nanofibers. *Sens. Actuators, B* **2009**, *137*, 471−475.
(50) Zeng, Y.; Zhang, T.; Wang, L.; Kang, M.; Fan, H.; Wang, R.; He, Y. Enhanced toluene sensing characteristics of $TiO_2$-doped flowerlike ZnO nanostructures. *Sens. Actuators, B* **2009**, *140*, 73−78.
(51) Aroutiounian, V. M.; Adamyan, Z. N.; sayunts, A. G.; Khachaturyan, E. A.; Adamyan, A. Z. Study of MWCNT/$SnO_2$ Nanocomposite Acetone and Toluene vapor Sensors. *Proceedings Sensor*, 2015; pp 836−841.
(52) Deng, L.; Ding, X.; Zeng, D.; Zhang, S.; Xie, C. High Sensitivity and Selectivity of C-Doped $WO_3$ Gas Sensors Toward Toluene and Xylene. *IEEE Sens. J.* **2012**, *12*, 2209−2214.
(53) Suematsu, K.; Watanabe, K.; Tou, A.; Sun, Y.; Shimanoe, K. Ultraselective toluene-gas sensor: Nanosized gold loaded on zinc oxide nanoparticles. *Anal. Chem.* **2018**, *90*, 1959−1966.
(54) Wang, L.; Deng, J.; Lou, Z.; Zhang, T. Nanoparticles-assembled Co3O4 nanorods p-type nanomaterials: One-pot synthesis and toluene-sensing properties. *Sens. Actuators, B* **2014**, *201*, 1−6.
(55) Yuan, T.; Li, Z.; Zhang, W.; Xue, Z.; Wang, X.; Ma, Z.; Fan, Y.; Xu, J.; Wu, Y. Highly sensitive ethanol gas sensor based on ultrathin


https://doi.org/10.1021/acsomega.1c01831
*ACS Omega* 2021, 6, 17442−17454

nanosheets assembled $Bi_2WO_6$ with composite phase. *Sci. Bull.* **2019**, *64*, 595−602.
(56) Xue, Z.; Yan, M.; Yu, X.; Tong, Y.; Zhou, H.; Zhao, Y.; Wang, Z.; Zhang, Y.; Xiong, C.; Yang, J.; Hong, X.; Luo, J.; Lin, Y.; Huang, W.; Li, Y.; Wu, Y. One-Dimensional Segregated Single Au Sites on Step-Rich ZnO Ladder for Ultrasensitive $NO_2$ Sensors. *Chem* **2020**, *6*, 3364−3373.



https://doi.org/10.1021/acsomega.1c01831
*ACS Omega* 2021, 6, 17442−17454